

## Chapter 4 Ion exchange of heavy metals using a modified zeolite filter integrated into a prototype autonomous water purifier (AWP) on a community scale

### Capítulo 4 Intercambio iónico de metales pesados mediante un filtro de zeolita modificado integrado en un prototipo de purificador de agua autónomo (PAA) a escala comunitaria

BECERRA-PANIAGUA, Dulce K.†\*, HERNÁNDEZ-GRANADOS, Araceli'', RUIZ SUAREZ, Alison''' and CEDANO-VILLAVICENCIO, Karla´

† *Instituto de Energías Renovables. Universidad Nacional Autónoma de México. Priv. Xochicalco S/N, 62580 Temixco, Morelos, México*

'' *Instituto de Ciencias Físicas, Universidad Nacional Autónoma de México, Av. Universidad 2001, Chamilpa 62210, Cuernavaca, México.*

''' *Instituto de Investigación e Innovación en Energías Renovables. Universidad de Ciencias y Artes de Chiapas. Libramiento Norte Poniente 1150, Col. Lajas Maciel, 29035, Tuxtla Gutiérrez, Chiapas, México.*

ID 1<sup>st</sup> Author: Dulce K., Becerra-Paniagua / **ORC ID:** 0000-0003-0471-7044, **CVU CONACYT ID:** 457428

ID 1<sup>st</sup> Co-author: Araceli, Hernández-Granados / **ORC ID:** 0000-0001-9439-5362, **CVU CONACYT ID:** 442077

ID 2<sup>nd</sup> Co-author: Alison, Ruiz-Suarez / **ORC ID:** 0000-0003-4694-8465, **CVU CONACYT ID:** 796976

ID 3<sup>rd</sup> Co-author: Karla, Cedano-Villavicencio / **ORC ID:** 0000-0002-8102-7226, **CVU CONACYT ID:** 84872

**DOI:** 10.35429/H.2021.16.53.69

D. Becerra, A. Hernández, A. Ruiz and K. Cedano

\* dkbp@ier.unam.mx

A. Marroquín, J. Olivares, D. Ventura, L. Cruz. (Coord.) CIERMMI Women in Science TXVI Engineering and Technology. Handbooks-©ECORFAN-México, Querétaro, 2021.

## Abstract

In Latin America and the Caribbean, the second leading cause of death is from diarrheal diseases. The main causes come from the consumption of water contaminated mainly by *Escherichia coli* (*E. coli*) and heavy metals, both associated with toxicity and bioaccumulation in living beings. In this chapter we study the exchange of ions of mercury ( $\text{Hg}^{2+}$ ), lead ( $\text{Pb}^{2+}$ ), cadmium ( $\text{Cd}^{2+}$ ) and copper ( $\text{Cu}^{2+}$ ) from aqueous solutions on an unmodified and modified clinoptilolite-K zeolite. To validate a prototype of the Autonomous Water Purifier (AWP) with the integrated zeolite filter, which helps solve problems in marginalized communities where they do not have access to drinking water, electricity and suffer from water-borne diseases. For this, adsorption and removal tests were carried out at different concentrations from 20 to 100 mg/l of heavy metals in aqueous solution with a certain amount of unmodified and modified zeolite. The recorded data represented by the Langmuir isotherm show that the metal ions  $\text{Hg}^{2+}$  and  $\text{Cu}^{2+}$  were exchanged very slightly, on the other hand, the metal ions of  $\text{Pb}^{2+}$  and  $\text{Cd}^{2+}$  were exchanged on the zeolites in greater quantity than the previous ions.

## Heavy metals removal, Water purification, Water treatment, Zeolite

### Resumen

En América Latina y el Caribe, la segunda causa de muerte es por enfermedades diarreicas. Las principales causas provienen del consumo de agua contaminada principalmente por *Escherichia coli* (*E. coli*) y metales pesados, ambos asociados a la toxicidad y bioacumulación en los seres vivos. En este capítulo se estudia el intercambio de iones de mercurio ( $\text{Hg}^{2+}$ ), plomo ( $\text{Pb}^{2+}$ ), cadmio ( $\text{Cd}^{2+}$ ) y cobre ( $\text{Cu}^{2+}$ ) de soluciones acuosas sobre una zeolita clinoptilolita-K sin modificar y modificada. Validar un prototipo de purificador de agua autónomo (AWP) con el filtro de zeolita integrado, que ayuda a resolver los problemas de las comunidades marginadas que no tienen acceso al agua potable ni a la electricidad y sufren enfermedades transmitidas por el agua. Para ello, se realizaron pruebas de adsorción y eliminación a diferentes concentraciones de 20 a 100 mg/l de metales pesados en solución acuosa con una determinada cantidad de zeolita no modificada y modificada. Los datos registrados representados por la isoterma de Langmuir muestran que los iones metálicos  $\text{Hg}^{2+}$  y  $\text{Cu}^{2+}$  se intercambiaron muy ligeramente, en cambio, los iones metálicos de  $\text{Pb}^{2+}$  y  $\text{Cd}^{2+}$  se intercambiaron en las zeolitas en mayor cantidad que los anteriores.

## Eliminación de metales pesados, Purificación del agua, Tratamiento del agua, Zeolita

### 4.1 Introduction

Today the shortage of safe water in the world has become a serious problem, since it affects thousands of people, mainly the vulnerable population in rural and remote areas. This problem does not arise from the "lack of water" in the area and even areas with high water resources are facing it. For example, Latin America and the Caribbean (LAC) are regions with high water resources, they have almost 34% of the world's fresh water (Mekonnen, Pahlow, Aldaya, Zarate, & Hoekstra, 2015). However, access to potable and purified water is insufficient and its quality is inadequate (Flachsbarth et al., 2015). According to the World Health Organization (WHO) and the United Nations International Children's Emergency Fund (UNICEF), around 2.2 billion people around the world do not have safe water services, which are managed safely, 4.2 billion people do not have safely managed sanitation services and 3 billion people lack basic facilities to wash their hands (UNICEF and World Health Organization, 2015, 2019). In addition, the COVID-19 pandemic has triggered serious alerts about these mentioned problems.

Lack of water is known to bring many social problems. For example, in 2017 almost 1.6 million people died from diarrheal diseases worldwide (WHO & UNICEF, 2017) and in Latin America and the Caribbean, it is the second leading cause of death (PAHO/WHO, 2019). Diarrheal disease is completely predictable and treatable and the main causes come from the consumption of water contaminated mainly by *Escherichia coli* (*E. coli*) and heavy metals (Jaishankar, Tseten, Anbalagan, Mathew, & Beeregowda, 2014), both associated with toxicity and bioaccumulation in living beings (Marazzato et al., 2020; Shaharoon et al., 2019).

In the case of Latin America and the Caribbean, 74.3% and 31.3% of the population respectively have access to safely managed water and sanitation services (Pan American Health Organization (PAHO), 2017). Mexico is one of the Latin American countries with the largest supply of fresh water in the world, each year Mexico receives around 1,449,471 million cubic meters of water in the form of precipitation. The North, Center and Northwest regions have 1/3 of the renewable water equivalent to 4/5 of the population (1,581.28 m<sup>3</sup>/inhab/year) which is less than the Southeast region, which has 2/3 of the renewable water equivalent to 1 / 5 of the population (10, 718.25 m<sup>3</sup> / inhab / year) (National Water Commission (NWC), 2017). Although the southeast region has more water, this region is the least developed in Mexico. The most affected states are Oaxaca, Guerrero, Campeche, and Chiapas. Among all these states, in 2016, the state of Chiapas had the highest renewable water resources per year and per capita in the country, 113,903 hm<sup>3</sup>/year and 21,419 m<sup>3</sup>/inhab/year, respectively (National Water Commission (NWC), 2017). Even with these water resources, most of the rural communities in this state do not have access to clean water, electricity and suffer from water-borne diseases.

Based on this situation and with the social problems mentioned above, it is convenient to work on the development of new concepts of water treatment systems that allow treating natural surface and underground waters with various pollutants, among the most alarming heavy metals. In addition, it is also important to use renewable energy as an energy supply for its operation. This, in order to be implemented in rural areas, helping to provide solutions to improve the quality of life and health of society.

For those reasons, this chapter is organized into the following sections: Introduction, describes a general panorama in Latin America and the Caribbean of the problems caused by contaminated water and its social impact; background, state of the art of the most used water treatment methods and zeolite as an adsorbent for pollutants, as well as the justification for the work; methodology, materials and methods used to evaluate zeolite with heavy metals and validate it in the Autonomous Water Purifier prototype (AWP); results and discussion, the results of the cation exchange modification of the zeolite are discussed, the study of the structural, morphological and chemical properties of the zeolites, the evaluation of the zeolites with heavy metals and the validation of this in a treatment system of water on a community scale. Finally, the conclusions, acknowledgments, and references are presented.

#### **4.1.1 Overview of contaminated water treatments**

In order to provide solutions to these types of problems, many lines of research have shown that household water treatment can be the most profitable option (Holtman, Haldenwang, & Welz, 2018; Murray et al., 2020). However, this method has a disadvantage, such as taste and poor disinfection efficiency. Other options are the use of solar radiation for the treatment of drinking water using SODIS (solar water disinfection) (Kohn, Mattle, Minella, & Vione, 2016; Parsa et al., 2020; Vivar, Pichel, & Fuentes, 2017); this method confirmed its effectiveness in eliminating bacteria, fungi and viruses. However, the time required for sun exposure is at least 6 hours; if it is cloudy, this is up to 2-3 days (Wang et al., 2016). In addition, in another article it was reported that to improve the efficiency of solar disinfection it was done by adding a photocatalyst, such as titanium dioxide (TiO<sub>2</sub>) (Fernández-Ibáñez et al., 2015; Wu et al., 2014). Although TiO<sub>2</sub> increased the effectiveness of SODIS, the TiO<sub>2</sub> nanoparticle suspension had to be separated before human consumption (otherwise it could be a risk to human health), and the process is expensive and difficult. Even with this great potential, SODIS is limited to disinfection efficiency and scale, because large-scale systems such as continuous flow or pump circulation need electricity and are no longer useful for rural and remote areas that lack of sanitation, water, and electricity. For these reasons, other works have developed photocatalytic-photovoltaic hybrid prototypes for the treatment of polluted water (Qin et al., 2015; Vivar et al., 2012). Other works reported the use of hybrid systems that use solar radiation, these systems were pilot-scale solar photoreactors, which included flat plate reactors (FPR) and compound parabolic collector (CPC) reactors (Ochoa-Gutiérrez, Tabares-Aguilar, Mueses, Machuca-Martínez, & Li Puma, 2018; Wang et al., 2016). Many hybrid systems have been developed for remote locations to desalinate water using reverse osmosis (Alghoul et al., 2016; Peng, Maleki, Rosen, & Azarikhah, 2018) and ultra-filtration membranes (Clayton, Thorn, & Reynolds, 2019).

The main advantage of hybrid systems is that they do not require conventional energy for their operation; therefore, it favors its implementation in remote areas that lack potable water and electricity. However, despite its great functionality, each method has its disadvantages, such as high cost, inappropriate taste, low scalability, and most importantly, low removal efficiency of toxic contaminants such as heavy metals (mercury, lead, arsenic, cadmium, and copper). Those studies only showed a low range of removal of contaminants such as dyes, salts, microorganisms.

On the other hand, in recent years zeolites have received a lot of attention in the scientific field for the removal of contaminants in water on a large scale. Zeolites are micro-porous aluminosilicate minerals that stand out for their ability to hydrate and dehydrate reversibly (Lin et al., 2013). The structure consists of a three-dimensional network of  $[\text{SiO}_4]^{-4}$  and  $[\text{AlO}_4]^{-5}$  tetrahedra, with the silicon or aluminum atoms in the center, and the oxygens at the vertices. The substitution of aluminum atoms for silicon in the crystal structure leads to the additional negative charge being balanced by adjacent counter ions (such as  $\text{Na}^+$ ,  $\text{K}^+$ ,  $\text{Ca}^{2+}$  and  $\text{Mg}^{2+}$  and these counterions are easily exchanged for other adjacent cations in an exchangeable solution (Dyer, 2007). In addition, zeolites have certain qualities and characteristics such as a high ion exchange and adsorption capacity (Kithome, Paul, Lavkulich, & Bomke, 1998). In Mexico, there are large deposits of rock rich in zeolites in the states of Sonora, San Luis Potosí, Guerrero, Tamaulipas, Puebla, Guanajuato, Oaxaca, Zacatecas and Baja California Sur (Cucchiella, D'Adamo, Lenny Koh, & Rosa, 2015) the current shortage of competitive minerals and the relatively low market price, make it optimal candidates, as ion exchangers in domestic and commercial water purification, and other applications (Y. Li, Li, & Yu, 2017) improve the ammonium adsorption capacity of zeolite, different methods of modifying it have been reported, among them, treatment with an exchangeable solution of sodium hydroxide (NaOH), hydrochloric acid (HCl) or sodium chloride (NaCl) (Kotoulas et al., 2019; Shi et al., 2017), microwave pretreatment (Lei, Li, & Zhang, 2008) and calcination (Liang & Ni, 2009). Being the method with interchangeable solutions where the highest adsorption capacity has been obtained (Ates, 2014).

Because of this situation, it is intended to improve the performance of these devices with the study and coupling of the zeolite material in one of the ion exchanges stages of the autonomous water purifier prototype (AWP). This material, by possessing certain qualities and characteristics of porosity, adsorption and ion exchange capacity make it an ideal material for the removal of heavy metals in water; and thus, obtain a wide range of pollutant removal compared to those of conventional solar and wind purifiers, helping to improve their quality and use. Therefore, in this chapter we show the results on: (1) the modification of zeolite by cationic exchange with NaCl, (2) the study of the structure, morphology and chemical composition of a natural and modified zeolite; (3) adsorption and removal tests at different concentrations from 20 to 100 mg/l of mercury ( $\text{Hg}^{2+}$ ), lead ( $\text{Pb}^{2+}$ ), cadmium ( $\text{Cd}^{2+}$ ) and copper ( $\text{Cu}^{2+}$ ) in aqueous solution with a certain amount of natural and modified zeolite; (4) the validation of the modified zeolite in the Autonomous Water Purifier (AWP) prototype. The recorded data represented by the Langmuir isotherm of ion exchange on zeolitic minerals revealed that the metal ions  $\text{Hg}^{2+}$  and  $\text{Cu}^{2+}$  were exchanged very slightly, on the other hand, the metal ions of  $\text{Pb}^{2+}$  and  $\text{Cd}^{2+}$  were exchanged on the zeolites in greater quantity than previous ions. And that the exchange capacity of the modified zeolite increases with respect to the unmodified one, thus increasing the number of exchangeable ions. In addition, those in the validation showed that the AWP prototype has a wide range of pollutant removal compared to equivalent water treatment systems in the same locations, and the electricity generated by the solar cells can be used to power the entire system. The prototype was evaluated with river and spring water from different rural communities in Chiapas, Mexico. The results indicate that the prototype it can eliminate pollutants in natural waters and obtaining water that complies with the guidelines established by the official Mexican standards.

## 4.2 Materials y methods

Next, the methodology used for the adsorption and ion exchange of mercury ( $\text{Hg}^{2+}$ ), lead ( $\text{Pb}^{2+}$ ), cadmium ( $\text{Cd}^{2+}$ ) and copper ( $\text{Cu}^{2+}$ ) ions on natural and modified zeolite is described. Throughout this section, the procedure, tools, and parameters used to achieve the planned objective are shown. Likewise, it describes the characteristics and conditioning of the type of zeolite that was used, the type of isotherm, the factors that were considered in the ionic exchange, the time in which they were stirred, at which temperature and pH were maintained. On the other hand, the techniques used for the characterization of materials and the technique used for the quantification of the equilibrium concentration of heavy metals in aqueous solution are described.

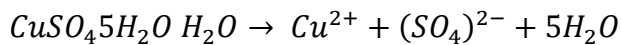
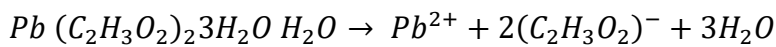
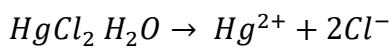
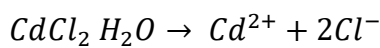
### 4.2.1 Experimental methodology

#### Stage 1. Conditioning of natural zeolite

A clinoptilolite-K type natural zeolite was used with a chemical composition of  $K_3(Si_3OAl_6)O_{72} \cdot 20H_2O$ , endemic to the Etna deposit (17° 12' 24" Norte, 96° 47' 53" West) of the state of Oaxaca. For this, a significant amount of the zeolite mineral was washed several times using deionized water, separated by decantation, dried for 24 hours in a Riossa H-33 oven at 110 °C (Figure 1.1a) and stored in closed containers and dry.

#### Stage 2. Preparation of exchangeable metal ion solutions

The precursors that were used to prepare the exchangeable solutions of the metal ions were the following inorganic salts:  $CdCl_2$ ;  $HgCl_2$ ;  $Pb(C_2H_3O_2)_2 \cdot 3H_2O$ ;  $Zn(NO_3)_2$ ;  $CuSO_4 \cdot 5H_2O$  due to its high degree of solubility in aqueous media. From the following hydrolysis chemical reactions, the amount in grams was determined despite the precursors to obtain concentrations of A=20, B=40, C=60, D=80 y F=100 mg/l of the metal ions.



#### Stage 3. Ion exchange isotherms

Since ion exchange is a form of adsorption, the experimental data of equilibrium of metal ions were interpreted by means of the Langmuir isotherm model, which are represented mathematically as (Mihaly-Cozmuta et al., 2014):

$$N = \frac{N_{max}KC}{1+KC} \quad (1)$$

Where: C is the concentration of metal ions at equilibrium, K is the Langmuir isotherm constant related to the enthalpy of adsorption, N is the amount of metal ion exchanged per unit mass of the adsorbent and  $N_{max}$  represents the maximum amount of  $Hg^{2+}$ ,  $Pb^{2+}$ ,  $Cd^{2+}$  y  $Cu^{2+}$  that is exchanged.

The data were adjusted to this model because it is the most used in adsorption phenomena at the solid-liquid interface on microporous materials such as zeolites. The isotherm constant was estimated using the least squares method by plotting the C/N ratio as a function of the equilibrium concentration C adjusting to a straight line of slope  $1/N_{max}$  and ordered to the origin  $1/KN_{max}$  for the Langmuir isotherm, using the following equation (Mihaly-Cozmuta et al., 2014):

$$\frac{C}{N} = \frac{C}{N_{max}} + \frac{1}{KN_{max}} \quad (2)$$

For the experiments with natural and modified zeolite, the experimental data of the exchange isotherm were obtained in a batch exchanger that consisted of a 500 ml Erlenmeyer flask, to which 500 ml of a solution containing an initial concentration of the ion were added. metallic from 20 to 100 mg/l. In a fabric made of nylon mesh, 26 g of zeolite were added in the form of a filter, as expressed in Figure 4.1 (b), then it was placed into the exchanger solution, as shown in Figure 4.1 (c).

#### Stage 4. Ion exchange kinetics

The solution was mixed by means of a Teflon coated magnetic stir bar and driven by a stir plate, as shown in Figure 1.1 (d). The solution and the zeolite were left in contact until they reached equilibrium at room temperature (25 °C) and 500 rpm.

It was found that in a period of 24 hours it is enough to reach equilibrium. This procedure was carried out for each exchangeable solution of the metal ion at five different concentrations, in total 25 samples were obtained. Which were stored in amber containers and kept at low temperatures, as shown in Figure 4.1 (d). To subsequently measure the concentration of the analyte in the solution by means of the Inductively Coupled Plasma Optical Emission (ICP-OES) technique, using a Thermo Scientific iCAP 6000 SERIES spectrometers.

*Stage 5. Modification of the zeolite by cation exchange (effect of pH)*

The process of modification by cationic exchange of zeolite has the purpose of replacing the cations that the natural mineral contains in its structure by sodium ions, coming from the sodium salt. The modification of the zeolite was carried out by a cation exchange procedure. 110 g of the natural zeolite and 200 ml of the exchangeable solution of NaCl at 2M were added to four 250 ml Erlenmeyer flasks. The solution and the zeolite were placed on a heating plate and heated to a temperature of 50 °C, the assembly can be seen in Figure 4.1 (e), for 12 h and then allowed to cool for the next 12 h; the exchangeable solution was separated from the zeolite by decantation. Next, 200 ml of a new exchangeable solution were added, and it was heated again to 50°C. This procedure was repeated for five days. At the end of this period the zeolite was separated from the solution, washed repeatedly with distilled water until the rinse solution was no longer cloudy, and dried in an oven at 110 ° C for 24 h. Hydrochloric acid (HCl) was used to adjust the initial pH from 7 to 5, because the maximum and optimal pH values for metal adsorption are reported to be between 5 and 6.5 (Elboughdiri, 2020). The modified zeolite was stored in a dry and closed container. The experimental data of the isotherm were obtained following the same procedure of the natural zeolite with the same conditions.

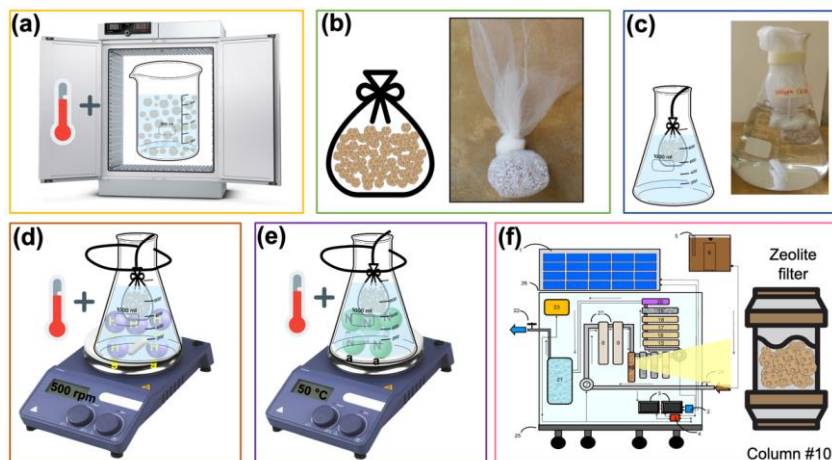
*Stage 6. Validation of zeolite as a filter in the Autonomous Water Purifier (AWP) prototype*

The ion exchange of heavy metals in aqueous solution in the zeolite column (10) was studied as shown in Figure 4.1 (f), of the Autonomous Water Purifier (AWP) prototype with patent registration number MX/a/2016/006341 (377936B, 2021). The absorbance of the final ion concentration was measured after being filtered by the AWP prototype using an ICP-OES spectrometer. The concentration was calculated by the calibration curve method, this process was carried out by establishing the calibration curve on standard metallic solutions at concentrations of 10 to 100 mg/ml.

The percentage of removal of metal cations (% R) was calculated from the difference in the concentration of initial metal cations ( $C_i$ ) and final ( $C_f$ ) in each sample, using the following equation (Erdem, Karapinar, & Donat, 2004).

$$\%R = \frac{C_i - C_f}{C_f} \times 100 \quad (3)$$

**Figure 4.1** Scheme of the natural and modified zeolite adsorption and ion exchange methodology: a) conditioning of natural zeolite, b) preparation of exchangeable metal ion solutions, c) ion exchange isotherms, d) ion exchange kinetics, e) modification of the zeolite by cation exchange (effect of pH) and, f) validation of zeolite as a filter in the Autonomous Water Purifier (AWP) prototype



## 4.2.2 Characterization

To study the effect of the cation exchange of the modified zeolite on the natural zeolite in the structural, morphological, and chemical properties, the following techniques and analyzes were used. The identification of the crystalline phases and the determination of the crystalline structure of the natural and modified zeolite samples were carried out by X-ray Diffraction (XRD). The equipment used was a Rigaku powder diffractometer, Ultima IV model, using radiation  $\text{CuK}\alpha$  ( $\lambda=1.54\text{\AA}$ ), operating at 40 kV and 44 mA. The samples were analyzed in a diffraction angle interval  $2\theta= 4-60^\circ$  with a step size of  $0.02^\circ$  and a span of 2 s. The data treatment was carried out with *Integrated X-Ray Powder Diffraction Software* (PDXL). The zeolite samples were ground in an agate mortar until obtaining a homogeneous fine powder. The morphological analysis of the natural and modified zeolite was carried out through the Scanning Electron Microscopy (SEM) technique, obtaining as a result, photomicrographs of the surfaces of the respective zeolites. A Jeol JSM-5300 scanning electron microscope (SEM) with tungsten filament, operating at 10 kV at a temperature of 298 K, was used to obtain the microphotographs of the surface morphology of the zeolites. To determine the chemical composition and the amount of metal cations adsorbed in the natural and modified zeolite samples, the X-Ray Fluorescence (XRF) technique was used. For this, a Rigaku brand spectrometer, model supermini 200, was used.

## 4.3 Results and discussion

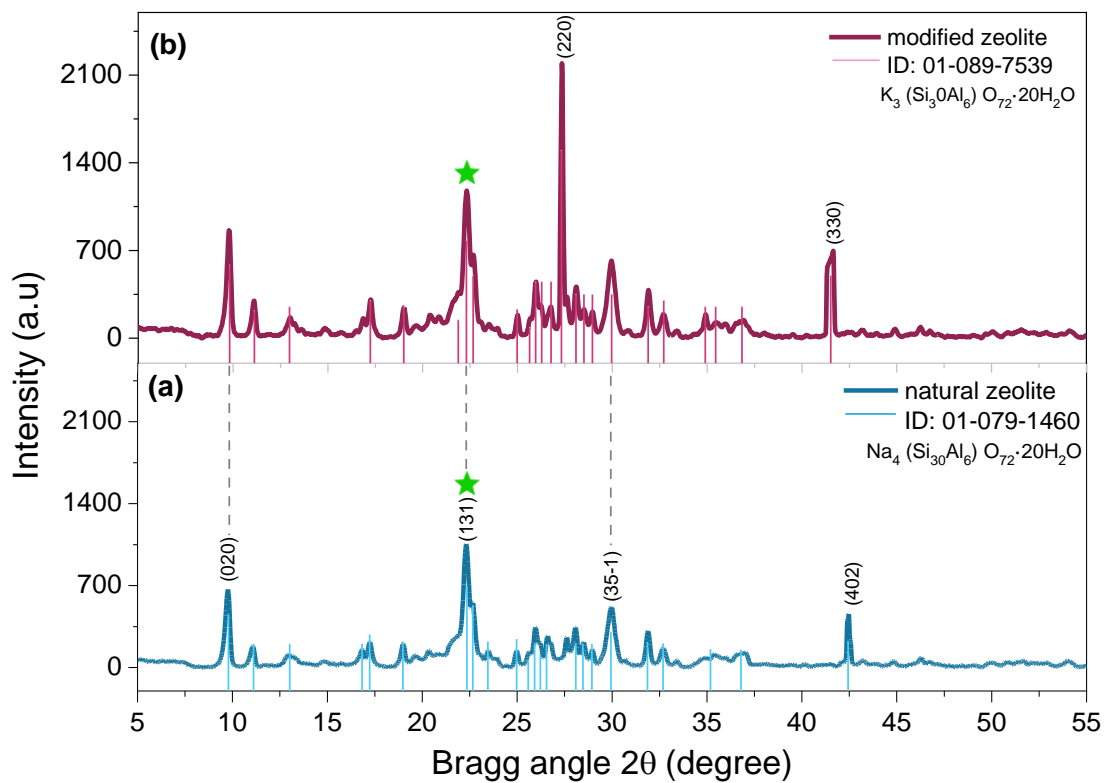
In this section, the results obtained from the characterization of the zeolite material with different techniques are presented. For that purpose, we analyze the effect of cation exchange on its structure, morphology, and chemical composition in zeolite; These techniques allowed us to know and deduce its porosity, ion exchange capacity, Si / Al ratio and the amount of metal ions exchanged and adsorbed on its surface. And thus, be able to conclude if said zeolite is efficient to remove heavy metals in water and decide on its validation as a material to be integrated into the Autonomous Water Purifier prototype (AWP). In addition, the evaluation of the zeolites on heavy metals, the graphs of ion exchange isotherms, the mass balance of exchanged ions, the removal percentages and the theoretical and experimental exchange capacity of the zeolites are presented; and the validation of the Autonomous Water Purifier prototype (AWP) with the integrated zeolite.

### 4.3.1 Structural analysis

The XRD technique allowed us to determine the crystalline phases of the material, which provides us with information about the type of zeolite and to verify if it is one of the 8 types of zeolites suitable for the removal of heavy metals; The crystal size allowed us to deduce its Silicon/Aluminum (Si/Al) ratio, which is a function of the ion exchange capacity of the zeolite.

Graphic 4.1 shows the X-ray diffraction spectra for natural and modified zeolite powders. Crystalline networks are observed in the monoclinic structure with a predominance of intensity and width of the peak in the plane of (131) of the reflection of natural zeolite and a predominance of intensity in the plane (220), and width of the peak (131) from the reflection of the modified zeolite. The diffractogram in Figure 4.1 (a) corresponds to the diffraction pattern ID: 01-089-7539,  $\text{K}_3(\text{Si}_{30}\text{Al}_6)\text{O}_{72}\cdot 20\text{H}_2\text{O}$ . The type of zeolite identified is a K-clinoptilolite phase. The most characteristic peaks are recognized at  $2\theta$  equal to  $9.87^\circ$ ,  $22.35^\circ$ ,  $29.94^\circ$  and  $42.42^\circ$ . The X-ray diffractogram from graphic 4.1, corresponds to the diffraction patterns of ID 01-079-1460,  $\text{Na}_4(\text{Si}_{30}\text{Al}_6)\text{O}_{72}\cdot 20\text{H}_2\text{O}$ . The zeolite type identified is a clinoptilolite-Na phase. The most characteristic peaks observed are located at  $2\theta$ , with values of  $9.84^\circ$ ,  $22.30^\circ$ ,  $27.31^\circ$  and  $41.52^\circ$ . Also, it is observed that in the modified zeolite, as the silicon/aluminum molar ratio decreases, the intensity of the diffractogram peaks increases, increasing their crystallinity due to the presence of the increase in sodium concentration, while the presence of potassium in the natural zeolite attenuates it.

**Graphic 4.1** X-ray diffractograms of (a) natural zeolite with the clinoptilolite-K pattern and (b) for modified zeolite with the clinoptilolite-Na pattern



Source: Elaborated by authors with Software Origin

By means of the patterns of natural and modified zeolite XRD, it was possible to obtain the crystallite size ( $D$ ), which shows the polycrystalline nature of zeolites. The realization of these calculations was conceived using the Debye-Scherrer equation, which establishes that the crystallite size is inversely proportional to the width of the peak at half the maximum diffraction height and the cosine of the maximum peak angle, according to the following formula:

$$D = \frac{K\lambda}{\beta \cos\theta} \quad (4)$$

Where  $\theta$  is the Bragg angle and  $\beta^2 = (FWHM)^2 - b^2$ ;  $FWHM$  is the full width at half the maximum peak of the sample,  $b$  instrumental error  $0.101^\circ$ ,  $\lambda = 1.54056 \text{ \AA}$  corresponds to the Cu  $K_\alpha$  radiation,  $D$  is the size of the crystallite,  $K$  is the shape factor that is approximately the unit of samples. Plane (131) was chosen as the representative of the samples and sizes obtained from Graphic 4.1. The crystallite size was  $327 \text{ \AA}$  with a 20% error for the natural zeolite and  $391 \text{ \AA}$  with a 22% error for the modified zeolite. By decreasing the Si / Al molar ratio in the zeolites, a tendency to form larger crystals is obtained, due to the presence of the increase in  $\text{Na}^+$  in their structure, favoring crystallinity in it.

### 4.3.2 Morphology analysis

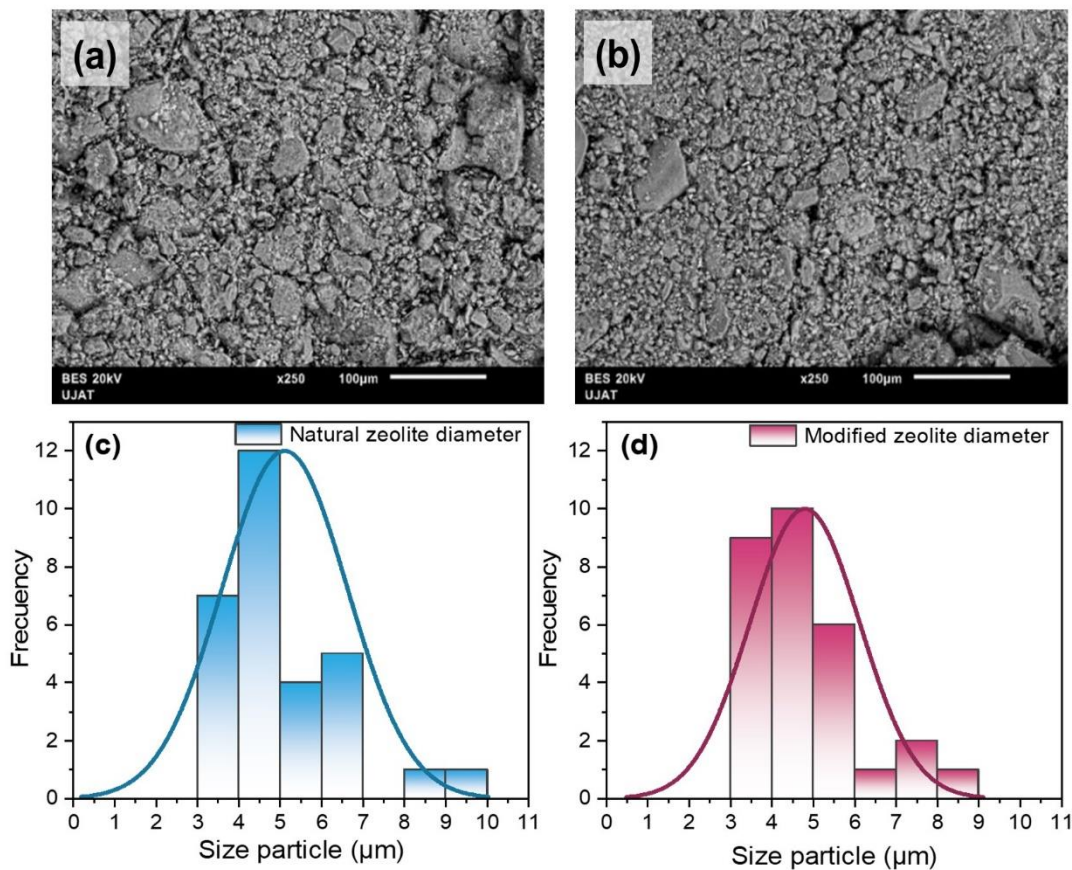
The SEM technique allowed obtaining information about the morphology, the particle size distribution, and the types of particle shapes that the natural and cation exchange modified zeolite samples presented, through visualization and microstructural analysis at a resolution of  $100 \mu\text{m}$ .

The zeolite samples presented four different types of particle shapes: angular-subangular-wavy, angular-smooth-wavy, subangular-rough and sub-round-wavy according to the literature (Li et al., 2019), whose variability is related to particle size and in turn to pore diameter. Larger particles, as in the case of natural zeolite, presented a greater variety in the types of shapes and greater distribution of the particles; while in the modified zeolite samples, because they had smaller particles, they presented a lower distribution of the particles and uniformity in the shapes of the particles. Figure 4.2 (a) shows the SEM image of the natural zeolite while Figure 4.2 (b) shows the SEM image of the cation exchange modified zeolite.



Particles were measured using ImageJ software from a section of the image; The area ( $\mu\text{m}^2$ ) of more than 40 particles was measured and for regular and two-dimensional particles we calculated their diameter ( $\mu\text{m}$ ), which we will call particle size, assuming a circular geometry ( $A=r^2\pi$ ). The natural and modified zeolite distributions are presented in Graphic 4.2 (c) and (d) respectively. A broader size distribution is observed for the natural zeolite sample, with diameters from  $3.0 \mu\text{m}$  to  $9.1 \mu\text{m}$  and an average of  $5.1 \pm 1.5 \mu\text{m}$ . In contrast, the modified zeolite sample has a shorter distribution, with diameters from  $3.2 \mu\text{m}$  to  $8.8 \mu\text{m}$  and an average of  $4.8 \pm 1.32 \mu\text{m}$ . The particles of a zeolite form three types of pores: packing, simple and cavities according to the literature (Anicua Sánchez et al., 2009); and have been determinate by Brunauer–Emmett–Teller (BET) and SEM techniques (Ramesh, Reddy, Rashmi, & Biswas, 2014). It can be established that the highest pore percentages are presented by the smaller sized particles, consequently the larger sized particles have a lower porosity percentage. Due to this, the zeolite conditioned with NaCl, by presenting smaller particle sizes compared to the natural zeolite, presented greater ion exchange and removal capacity, as will be seen later, by increasing its channels and cavities that vary according to size. particle. Therefore, metal cations in aqueous solution will more easily penetrate the crystal structure through their series of intersecting channels.

**Graphic 4.2** SEM images of samples of (a) natural zeolite and (b) modified zeolite; (c and d) particle size distribution of natural zeolite and modified zeolite respectively



Source: Elaboration by authors with Software Origin; SEM images acquired from Jeol JSM-5300

### 4.3.3 Chemical composition analysis

The XRF technique allowed to determine the elemental chemical composition and the ion exchange capacity as a function of the Si/Al ratio of the natural and modified zeolite; the results obtained are shown in Table 4.1.

**Table 4.1** Elemental composition of natural and modified zeolite, in percent by weight (wt%)

Zeolite samples	Molar ratio Si/Al	SiO <sub>2</sub> (wt%)	Al <sub>2</sub> O <sub>3</sub> (wt%)	Na <sub>2</sub> O (wt%)	MgO (wt%)	K <sub>2</sub> O (wt%)	CaO (wt%)	Fe <sub>2</sub> O <sub>3</sub> (wt%)
Natural	4.63	68.877	14.862	1.840	0.990	7.806	3.384	2.237
Modified	4.30	64.668	15.026	10.970	0.798	5.402	0.365	2.767

The unmodified zeolite is the one with the lowest ion exchange capacity, Si/Al= 4.63, this capacity is directly related to the aluminum present in the zeolite crystal lattice and depends directly on its chemical composition. The exchange capacity was modified by varying the silicon-aluminum ratio of the zeolite, increasing as this ratio decreased. For this, once the mineral was conditioned with NaCl, an increase of approximately 10 times the amount of sodium was obtained compared to the content of said element in the unconditioned mineral.

A high ion exchange capacity corresponds to zeolites with a low ratio  $\text{SiO}_2/\text{Al}_2\text{O}_3$ , or ratio Si/Al as is the case of modified zeolite, which was equal to 4.30. This ratio determined the number of cations that can be interchangeable in the zeolite, since by changing the Si / Al ratio of a zeolite, its cation content also changed.

#### 4.3.4 Evaluation of heavy metals on zeolites

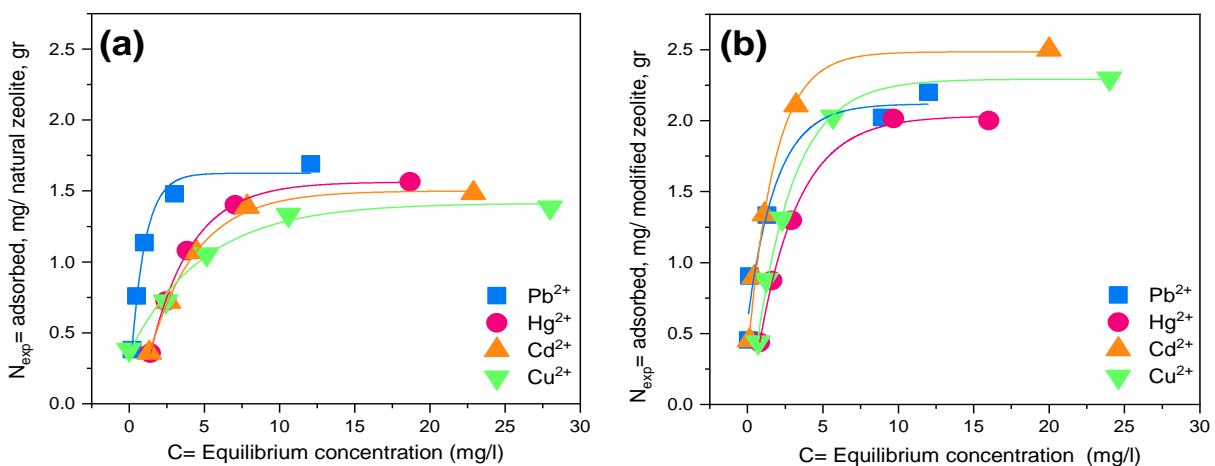
Considering the analytical technique of composition of analytes in aqueous solution mentioned in the methodology section, in Graphic 4.3 (a) and (b) the results of the adsorption and ion exchange of the experiment with natural zeolite and modification are summarized. The equilibrium concentrations (C) registered in the ICP-OES equipment of the metal ions in aqueous solution are represented against the amount of metal ion adsorbed per gram of experimental zeolite ( $N_{exp}$ ) calculated by the following equation:

$$N_{exp} = V_s * \frac{C_0 - C}{m_z} \quad (5)$$

The experimental data of the exchange isotherms of  $\text{Hg}^{2+}$ ,  $\text{Pb}^{2+}$ ,  $\text{Cd}^{2+}$  y  $\text{Cu}^{2+}$  on the natural and modified zeolite at  $T=25^\circ\text{C}$  and with adjustment of  $\text{pH}=5$ , were interpreted by means of the model of the Langmuir isotherm represented in the Graphic 4.3. The results of the ion exchange isotherms reveal that the metal ions  $\text{Pb}^{2+}$  y  $\text{Hg}^{2+}$  were the ones that were exchanged in greater quantity on the natural zeolite, obtaining the highest concentrations of 1.69 mg/gr and 1.56 mg/gr respectively at 100 mg/l. This is caused by the concentration of the related exchangeable cations  $\text{K}^+$  and  $\text{Ca}^{2+}$  present in greater quantity in the natural zeolite, 7.80 wt% and 3.38 wt% respectively.

On the other hand, the  $\text{Cd}^{2+}$  and  $\text{Cu}^{2+}$  metal ions exchanged very slightly on the natural zeolite, this caused by the low concentration of exchangeable related cations  $\text{Na}^+$  present in the natural zeolite samples of approximately 1.840 wt%. Other important results were on the modified zeolite samples, the metal ions  $\text{Cd}^{2+}$  and  $\text{Cu}^{2+}$  were the ones that were exchanged in greater quantity on this zeolite, obtaining the highest concentrations of 2.10 mg/ gr and 2.030 mg/gr respectively at 100 mg/l. This is due to the concentration of the affinity exchangeable cation  $\text{Na}^+$  present in greater quantity in the modified zeolite of 10.97 wt%. On the other hand, the metal ions  $\text{Pb}^{2+}$  and  $\text{Hg}^{2+}$  exchanged very slightly on the modified zeolite, this caused by the low concentration of exchangeable related cations  $\text{K}^+$  and  $\text{Ca}^{2+}$  present in the modified zeolite samples of 5.40 wt% and 0.36 wt% respectively.

**Graphic 4.3** Ion exchange isotherm of  $\text{Pb}^{2+}$ ,  $\text{Hg}^{2+}$ ,  $\text{Cd}^{2+}$  and  $\text{Cu}^{2+}$  on (a) natural zeolite and (b) modified zeolite



Source: Elaboration by authors with Software Origin; data obtained from the ICP-OES equipment

The isotherm constants were estimated using the least squares method of equation (2), plotting the C/N ratio as a function of the equilibrium concentration C for each metal ion. To obtain the constant of each isotherm,  $N_{max}$ , the value of the slope was cleared for each line of natural and modified zeolite of each metal ion:  $m = \frac{1}{N_{max}}$ . The values of the constant of each isotherm are shown in Table 4.2.

In addition, the average deviation percentage (% D) for each isotherm was evaluated using the following equation:

$$\%D = \left( \frac{1}{n} \sum_{i=1}^n \left| \frac{N_{exp} - N_{cal}}{N_{exp}} \right| \right) \times 100\% \quad (6)$$

It was considered that the natural zeolite isotherms were the ones that best fit the data, since in all cases they presented a lower percentage of deviation compared to the results of the percentage of deviation of modified zeolite. The explanation for this behavior is based on the variation of basicity and pH of the natural zeolite in the experiments. Caused that the ion exchange is slightly different. The exchange equilibrium is affected by the modification of NaCl on the natural zeolite causing variations that cause deviations in the data of the exchange isotherm. On the other hand, the results indicate that the metal ion  $Pb^{2+}$  and  $Cu^{2+}$  has the highest maximum amount of mg of metal ion that can be adsorbed on one gram of natural and modified zeolite, respectively. While  $Cu^{2+}$  and  $Hg^{2+}$  have the lowest maximum amount of mg of metal ion that can be adsorbed in a gram of natural and modified zeolite respectively.

**Table 4.2** Values of the Langmuir isotherm constant

Ion	Zeolite	$N_{max}$ (mg/gr)	%D
$Pb^{2+}$	Natural	1.785	3.33
$Hg^{2+}$		1.769	8.96
$Cd^{2+}$		1.753	10.73
$Cu^{2+}$		1.446	9.11
$Cd^{2+}$	Modified	2.610	11.20
$Cu^{2+}$		2.559	9.80
$Pb^{2+}$		2.349	27.81
$Hg^{2+}$		2.227	8.54

Source: Prepared by authors

In addition, the adsorbed and exchanged metal ions were quantified in each of the zeolite samples. To obtain the balance of the maximum metal ions exchanged on the surface of the zeolite mass, the  $N_{max}$  values already calculated and recorded in Table 4.2 were taken, and each value was multiplied by the mass of zeolite used (26 gr for natural zeolite and 22 gr for modified zeolite) to have the total mg exchanged of each metal ion on the surface of natural and modified zeolite. Regarding the balance of the metal ions adsorbed on the surface of the zeolite mass, they were obtained from the compositional characterization by the XRF technique, the team gave the results in percentage by mass and through calculations it was converted to mass units of mg.

The results of the mass balance of the metal ions that were exchanged, and the mass of the metal ions adsorbed in the natural and modified zeolite samples are shown in Table 4.3.

**Table 4.3** Mass balance of adsorbed and exchanged ions during ion exchange

Initial concentration (mg/l)	Zeolite	Ions adsorbed on the zeolite (mg)				Ions exchanged in zeolite (mg)			
		$Pb^{+2}$	$Hg^{+2}$	$Cd^{+2}$	$Cu^{+2}$	$Pb^{+2}$	$Hg^{+2}$	$Cd^{+2}$	$Cu^{+2}$
100	Natural	31.5	25.3	24.4	21.5	46.4	45.9	45.5	37.5
100	Modified	35.3	31.8	39.3	37.8	51.6	48.4	57.4	56.2

Source: Prepared by authors

The total ions that are transferred from the solution to the zeolite ( $\text{Pb}^{2+}$ ,  $\text{Hg}^{2+}$ ,  $\text{Cd}^{2+}$  and  $\text{Cu}^{2+}$ ) do not correspond to the total ions that are adsorbed from the solution to the zeolite. Since the zeolite operates as an exchanger and adsorber at the same time. The sum of the adsorbed ions and the exchanged ions gives us the total amount of the ion that was removed through the zeolite. It can be observed that the ion most exchanged and adsorbed was  $\text{Pb}^{2+}$  and  $\text{Cd}^{2+}$  on natural and modified zeolite, respectively. This means that clinoptilolite is much more selective for  $\text{Pb}^{2+}$  and  $\text{Cd}^{2+}$  ions than for  $\text{Hg}^{2+}$  and  $\text{Cu}^{2+}$  ions.

#### 4.3.4 Application of zeolite filter in the Autonomous Water Purifier prototype (AWP)




In Graphic 4.4 (a), the removal percentage (% R) is shown against the initial concentration ( $C_i$ ), while in Graphic 4.4 (b) the final concentration ( $C_f$ ) is shown against  $C_i$  of heavy metals in the zeolite ion exchange column (Figure 4.1f, column 10) in the AWP prototype, obtained by equation (3) and the ICP-OES equipment respectively. The curves were fitted with the following mathematical equation by exponential model:

$$y = y_0 + Ae^{bx} \quad (7)$$

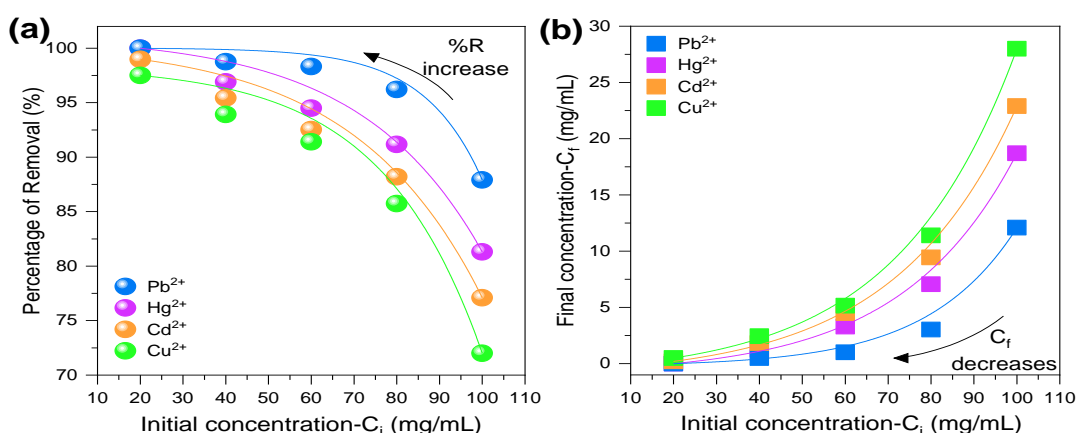
The removal rate of a cation in aqueous solution depends on the amount exchanged in the zeolite ion exchange column (column 10), as well as on the function of ion exchange. Thus, it was considered that, under the same experimental conditions, the sample that has a greater ionic exchange capacity is the one that exhibits the highest removal percentage for that ionic capacity (Erdem et al., 2004; Mihaly-Cozmuta et al., 2014).

In Graphic 4.4 (a) and (b), it can be observed that the %R and  $C_f$  decrease as the initial concentration of the metal increases in aqueous solutions, since the zeolite has a maximum adsorption capacity and tends to become saturated at high concentrations. The % R ranged from 87 to 99% for  $\text{Pb}^{2+}$ , 81 to 99% for  $\text{Hg}^{2+}$ , 77 to 98% for  $\text{Cd}^{2+}$  and 72 to 97% for  $\text{Cu}^{2+}$ . Comparing the %R obtained from the zeolite ion exchange column (10) for each metal, it is observed that the exchange selectivity in the zeolite is  $\text{Pb}^{2+} > \text{Hg}^{2+} > \text{Cd}^{2+} > \text{Cu}^{2+}$ , that is, that for the natural zeolite the  $\text{Pb}^{2+}$  is exchanged in greater quantity than the metal  $\text{Hg}^{2+}$  and thus for the metals  $\text{Cd}^{2+}$  and  $\text{Cu}^{2+}$ .

This cationic exchange can be attributed to the substitution of the exchangeable ions  $\text{Na}^+$ ,  $\text{Ca}^{2+}$  and  $\text{K}^+$  that constitute the zeolite with the divalent cations of  $\text{Pb}^{2+}$ ,  $\text{Hg}^{2+}$ ,  $\text{Cd}^{2+}$  and  $\text{Cu}^{2+}$ . This isomorphic substitution is due to the similarity in their ionic radius that metal cations have with exchangeable ions, the affinity of the dimensions in their cavities of the zeolite makes one cation take the place of the other, by simple interaction between their chemical bonds. Due to the similarity between their ionic radius, the replacement is concluded as follows (Shannon, 1976).

	Ion exchange	
$\text{K}^+$ (138 pm)		$\text{Pb}^{2+}$ (119 pm)
$\text{Ca}^{2+}$ (100 pm)		$\text{Hg}^{2+}$ (102 pm); $\text{Cd}^{2+}$ (95 pm)
$\text{Na}^+$ (102 pm)		$\text{Hg}^{2+}$ (102 pm)

**Graphic 4.4** (a) Percentage of removal (circles) and (b) final concentration (squares) of  $\text{Pb}^{2+}$ ,  $\text{Hg}^{2+}$ ,  $\text{Cd}^{2+}$  and  $\text{Cu}^{2+}$  in the zeolite ion exchange column as a function of the initial concentration.



Source: Elaboration by authors in Software Origin; data obtained from the ICP-OES equipment

The literature indicates that, in the case of metal cations and natural zeolites, the predominant mechanism is ion exchange. It can be assumed that the zeolite had a higher amount of exchangeable  $K^+$  ions, therefore, the highest exchange occurred with the  $Pb^{2+}$  cation. Final concentrations were 12.09 to 0.002 mg/ml for  $Pb^{2+}$ , 18.7 to 0.002 mg/ml for  $Hg^{2+}$ , 22.9 to 0.204 mg/ml for  $Cd^{2+}$  and 28 to 0.5 mg/ml for  $Cu^{2+}$  at an initial concentration of 100 to 20 mg/ml. The latest values at 20 mg/ml starting concentration are within the permissible limits for purified water according to OMS guidelines which are 0.01 mg/ml, 0.006 mg/ml, 0.003 mg/ml, and 2.00 mg/ml for  $Pb^{2+}$ ,  $Hg^{2+}$ ,  $Cd^{2+}$  and  $Cu^{2+}$  respectively.

These results indicate that the AWP prototype was designed to remove the major heavy metals to the permissible limits of the zeolite ion exchange column. The absorption of heavy metals is attributed to different mechanisms of the ion exchange processes, as well as the adsorption process. During the ion exchange process, the metal cations had to move through the pores of the zeolite and the channels of the network, which in turn replaced the exchangeable cations (mainly  $Na^+$ ,  $Ca^{2+}$  and  $K^+$ ). In this case, the uptake of metal ions could be attributed mainly to ion exchange reactions in the microporous minerals of the zeolite ion exchange column.

#### 4.4 Conclusions

As a result of the structural, morphological, and chemical composition characterizations carried out on natural zeolite and zeolite modified by cationic exchange, we can conclude that:

The type of natural and NaCl-conditioned zeolite was successfully identified, as well as the crystal size of each type of sample using the XRD technique. Clinoptilolite-K crystalline phase predominates for natural zeolite and clinoptilolite-Na for modified zeolite with a crystal size range of 327 a 391 Å. The SEM technique allowed obtaining morphological information of the samples, which revealed the distribution and shapes of the particles presenting four types: angular-subangular-wavy, angular-smooth-wavy, subangular-rough, and sub-round-wavy. With diameters from 3.0  $\mu m$  to 9.1 and an average of  $5.1 \pm 1.5 \mu m$  for the natural zeolite and for the modified zeolite sample, it presented a shorter distribution, with diameters from 3.2  $\mu m$  to 8.8  $\mu m$  and an average of  $4.8 \pm 1.32 \mu m$ . From the XRF technique it was possible to know the chemical composition and the ion exchange capacity as a function of the Si/Al ratio of each type of zeolite. This relationship indicates that natural zeolite has an ion exchange capacity, Si/Al= 4.63. By conditioning the natural zeolite with NaCl by cation exchange, it was possible to increase the ion exchange capacity, Si/Al= 4.30, increasing the amount of the exchangeable sodium ion approximately 10 times that of the original sample. A high ion exchange capacity corresponds to zeolites with a low Si/Al ratio.

As a result of the evaluation of the natural and modified zeolite by cationic exchange in aqueous solution with heavy metals, we can conclude that:

The recorded data represented by the Langmuir isotherm of ion exchange on the minerals revealed that the metal ions  $Hg^{2+}$  and  $Cu^{2+}$  were exchanged very slightly. On the other hand, the metal ions of  $Pb^{2+}$  and  $Cd^{2+}$  were exchanged on the zeolites in greater quantity than the other ions. In addition, the increasing order of the selectivity of the zeolites for the metal ions was reported, which was:  $Pb^{2+} > Hg^{2+} > Cd^{2+} > Cu^{2+}$  for the natural resin and  $Cd^{2+} > Cu^{2+} > Pb^{2+} > Hg^{2+}$  for the modified resin. This means that for the natural resin,  $Pb^{2+}$  is exchanged in greater quantity than  $Hg^{2+}$  and for modified resin,  $Cd^{2+}$  is exchanged in greater quantity than  $Cu^{2+}$  and so on. The theoretical exchange capacity ranged from 2.789 to 3.202 mg Al/gr and the decreasing order of the theoretical exchange capacity of the zeolite samples is as follows: conditioned zeolite > natural zeolite. This is because the amount of aluminum in these zeolites decreases in the same order. The experimental exchange capacity ranged from 1.785 to 2.349 mg/gr for  $Pb^{2+}$  ions, from 1.769 to 2.227 mg/gr for  $Hg^{2+}$  ions, from 1.753 to 2.610 mg/gr for  $Cd^{2+}$  ions and from 1.446 to 2.559 mg/gr for  $Cu^{2+}$  ions. The natural zeolite presented a higher exchange capacity for the  $Pb^{2+}$  ion and the modified zeolite for the  $Cd^{2+}$  ion. The experimental exchange capacity is less than the theoretical exchange capacity because not all active sites are accessible to cations and not all exchangeable cations present in zeolites can be exchanged.

The zeolite filter as a prototype Autonomous Water Purifier (AWP) reveals that the autonomous purifier is suitable and ideal for treating water from different sources, with high concentrations of heavy metals. Obtaining because of the purification process a clean, healthy, and suitable water for human consumption, with a good taste, smell, and color. Reducing gastrointestinal diseases and mortality rates in children transmitted by the consumption of this contaminated resource. Ensuring the health of society in rural areas where they lack quality of life and potable, purified water, and electricity services.

#### 4.5 Acknowledgments

The author and co-authors are grateful for the technical and financial support of Dr. Joel Pantoja Enríquez from the Instituto de Investigación e Innovación en Energías Renovables (IIER)- Universidad de Ciencias y Artes de Chiapas (UNICACH). Dr. Joel Moreira and Dr. Guillermo Ibáñez Duhart for their comments and discussion. To Erick Alejandro Hernández Domínguez for his support with the experiments. To the Instituto Tecnológico Nacional de México Campus Tuxtla Gutiérrez (ITTG) for their support with the ICP-OES characterization technique, as well Dr. Rocío Meza Gordillo for the understanding of this technique. The Universidad Juárez Autónoma de Tabasco for their support with the SEM characterization technique. Consejo Nacional de Ciencia y Tecnología (CONACyT-México) for the master and PhD scholarship given to DKBP, Dirección General de Asuntos del Personal Académico (DGAPA) for the postdoctoral scholarship of AHG. And finally, to the Instituto de Ciencia, Tecnología e Innovación del Estado de Chiapas (ICTI) for the financial support granted for the publication of this chapter.

#### 4.6 References

- Alghoul, M. A., Poovanaesvaran, P., Mohammed, M. H., Fadhil, A. M., Muftah, A. F., Alkilani, M. M., & Sopian, K. (2016). Design and experimental performance of brackish water reverse osmosis desalination unit powered by 2 kW photovoltaic system. *Renewable Energy*, *93*, 101–114. <https://doi.org/10.1016/j.renene.2016.02.015>
- Anicua Sánchez, R., Del Carmen Gutiérrez Castorena, M., Sánchez García, P., Ortiz Solorio, C., Volke Halle, V. H., Enrique, J., & Panta, R. (2009). Particle size and micromorphological relation on physical properties of perlite and zeolite, *35*, 147–156.
- Ates, A. (2014). Role of modification of natural zeolite in removal of manganese from aqueous solutions. *Powder Technology*, *264*, 86–95. <https://doi.org/10.1016/j.powtec.2014.05.023>
- Clayton, G. E., Thorn, R. M. S., & Reynolds, D. M. (2019). Development of a novel off-grid drinking water production system integrating electrochemically activated solutions and ultrafiltration membranes. *Journal of Water Process Engineering*, *30*(August 2017), 100480. <https://doi.org/10.1016/j.jwpe.2017.08.018>
- Cucchiella, F., D'Adamo, I., Lenny Koh, S. C., & Rosa, P. (2015). Recycling of WEEE: An economic assessment of present and future e-waste streams. *Renewable and Sustainable Energy Reviews*, *51*, 263–272. <https://doi.org/10.1016/j.rser.2015.06.010>
- Dyer, A. (2007). Natural Zeolites by G. V. Tsitsishvili, T. G. Andronikashvili, G. R. Kirov and L. D. Filizova. Ellis Horwood, Chichester 1991. No. of pages: 297. Price: £69.00 (hardback). ISBN 0 13 612037 7. *Geological Journal*, *29*(2), 192–192. <https://doi.org/10.1002/gj.3350290217>
- Elboughdiri, N. (2020). The use of natural zeolite to remove heavy metals Cu (II), Pb (II) and Cd (II), from industrial wastewater. *Cogent Engineering*, *7*(1). <https://doi.org/10.1080/23311916.2020.1782623>
- Erdem, E., Karapinar, N., & Donat, R. (2004). The removal of heavy metal cations by natural zeolites. *Journal of Colloid and Interface Science*, *280*(2), 309–314. <https://doi.org/10.1016/j.jcis.2004.08.028>
- Fernández-Ibáñez, P., Polo-López, M. I., Malato, S., Wadhwa, S., Hamilton, J. W. J., Dunlop, P. S. M., ... Byrne, J. A. (2015). Solar photocatalytic disinfection of water using titanium dioxide graphene composites. *Chemical Engineering Journal*, *261*, 36–44. <https://doi.org/10.1016/j.cej.2014.06.089>



- Flachsbarth, I., Willaarts, B., Xie, H., Pitois, G., Mueller, N. D., Ringler, C., & Garrido, A. (2015). The role of Latin America's land and water resources for global food security: Environmental trade-offs of future food production pathways. *PLoS ONE*, *10*(1), 1–24. <https://doi.org/10.1371/journal.pone.0116733>
- Holtman, G. A., Haldenwang, R., & Welz, P. J. (2018). Biological sand filter system treating winery effluent for effective reduction in organic load and pH neutralisation. *Journal of Water Process Engineering*, *25*(July), 118–127. <https://doi.org/10.1016/j.jwpe.2018.07.008>
- Jaishankar, M., Tseten, T., Anbalagan, N., Mathew, B. B., & Beeregowda, K. N. (2014). Toxicity, mechanism and health effects of some heavy metals. *Interdisciplinary Toxicology*, *7*(2), 60–72. <https://doi.org/10.2478/intox-2014-0009>
- Kithome, M., Paul, J. W., Lavkulich, L. M., & Bomke, A. A. (1998). Kinetics of Ammonium Adsorption and Desorption by the Natural Zeolite Clinoptilolite. *Soil Science Society of America Journal*, *62*(3), 622–629. <https://doi.org/10.2136/sssaj1998.03615995006200030011x>
- Kohn, T., Mattle, M. J., Minella, M., & Vione, D. (2016). A modeling approach to estimate the solar disinfection of viral indicator organisms in waste stabilization ponds and surface waters. *Water Research*, *88*, 912–922. <https://doi.org/10.1016/j.watres.2015.11.022>
- Kotoulas, A., Agathou, D., Triantaphyllidou, I. E., Tatoulis, T. I., Akratos, C. S., Tekerlekopoulou, A. G., & Vayenas, D. V. (2019). Zeolite as a potential medium for ammonium recovery and second cheese whey treatment. *Water (Switzerland)*, *11*(1). <https://doi.org/10.3390/w11010136>
- Lei, L., Li, X., & Zhang, X. (2008). Ammonium removal from aqueous solutions using microwave-treated natural Chinese zeolite. *Separation and Purification Technology*, *58*(3), 359–366. <https://doi.org/10.1016/j.seppur.2007.05.008>
- Li, S., Li, J., Dong, M., Fan, S., Zhao, T., Wang, J., & Fan, W. (2019). Strategies to control zeolite particle morphology. *Chemical Society Reviews*, *48*(3), 885–907. <https://doi.org/10.1039/C8CS00774H>
- Li, Y., Li, L., & Yu, J. (2017, December 14). Applications of Zeolites in Sustainable Chemistry. *Chem.* Elsevier Inc. <https://doi.org/10.1016/j.chempr.2017.10.009>
- Liang, Z., & Ni, J. (2009). Improving the ammonium ion uptake onto natural zeolite by using an integrated modification process. *Journal of Hazardous Materials*, *166*(1), 52–60. <https://doi.org/10.1016/j.jhazmat.2008.11.002>
- Lin, L., Lei, Z., Wang, L., Liu, X., Zhang, Y., Wan, C., ... Tay, J. H. (2013). Adsorption mechanisms of high-levels of ammonium onto natural and NaCl-modified zeolites. *Separation and Purification Technology*, *103*, 15–20. <https://doi.org/10.1016/j.seppur.2012.10.005>
- Marazzato, M., Aleandri, M., Massaro, M. R., Vitanza, L., Conte, A. L., Conte, M. P., ... Longhi, C. (2020). Escherichia coli strains of chicken and human origin: Characterization of antibiotic and heavy-metal resistance profiles, phylogenetic grouping, and presence of virulence genetic markers. *Research in Veterinary Science*, *132*(June), 150–155. <https://doi.org/10.1016/j.rvsc.2020.06.012>
- Mekonnen, M. M., Pahlow, M., Aldaya, M. M., Zarate, E., & Hoekstra, A. Y. (2015). Sustainability, efficiency and equitability of water consumption and pollution in latin America and the Caribbean. *Sustainability (Switzerland)*, *7*(2), 2086–2112. <https://doi.org/10.3390/su7022086>
- Mihaly-Cozmuta, L., Mihaly-Cozmuta, A., Peter, A., Nicula, C., Tutu, H., Silipas, D., & Indrea, E. (2014). Adsorption of heavy metal cations by Na-clinoptilolite: Equilibrium and selectivity studies. *Journal of Environmental Management*, *137*, 69–80. <https://doi.org/10.1016/j.jenvman.2014.02.007>
- Murray, A. L., Napotnik, J. A., Rayner, J. S., Mendoza, A., Mitro, B., Norville, J., ... Lantagne, D. S. (2020). Evaluation of consistent use, barriers to use, and microbiological effectiveness of three prototype household water treatment technologies in Haiti, Kenya, and Nicaragua. *Science of the Total Environment*, *718*, 134685. <https://doi.org/10.1016/j.scitotenv.2019.134685>

National Water Commission (NWC). (2017). Statistics on Water in Mexico, (November), 292.

Ochoa-Gutiérrez, K. S., Tabares-Aguilar, E., Mueses, M. Á., Machuca-Martínez, F., & Li Puma, G. (2018). A Novel Prototype Offset Multi Tubular Photoreactor (OMTP) for solar photocatalytic degradation of water contaminants. *Chemical Engineering Journal*, 341(July 2017), 628–638. <https://doi.org/10.1016/j.cej.2018.02.068>

PAHO/WHO. (2019). Nearly 16 million people still practice open defecation in Latin America and the Caribbean. Retrieved from [https://www3.paho.org/hq/index.php?option=com\\_content&view=article&id=15601:nearly-16-million-people-still-practice-open-defecation-in-latin-america-and-the-caribbean&Itemid=1926&lang=en](https://www3.paho.org/hq/index.php?option=com_content&view=article&id=15601:nearly-16-million-people-still-practice-open-defecation-in-latin-america-and-the-caribbean&Itemid=1926&lang=en)

Pan American Health Organization (PAHO). (2017). *Health in the Americas+, 2017 Edition. Summary: Regional Outlook and Country Profiles*.

Parsa, S. M., Rahbar, A., Koleini, M. H., Davoud Javadi, Y., Afrand, M., Rostami, S., & Amidpour, M. (2020). First approach on nanofluid-based solar still in high altitude for water desalination and solar water disinfection (SODIS). *Desalination*, 491(June), 114592. <https://doi.org/10.1016/j.desal.2020.114592>

Peng, W., Maleki, A., Rosen, M. A., & Azarikhah, P. (2018). Optimization of a hybrid system for solar-wind-based water desalination by reverse osmosis: Comparison of approaches. *Desalination*, 442(November 2017), 16–31. <https://doi.org/10.1016/j.desal.2018.03.021>

Qin, L., Wang, Y., Vivar, M., Huang, Q., Zhu, L., Fuentes, M., & Wang, Z. (2015). Comparison of photovoltaic and photocatalytic performance of non-concentrating and V-trough SOLWAT (solar water purification and renewable electricity generation) systems for water purification. *Energy*, 85, 251–260. <https://doi.org/10.1016/j.energy.2015.03.106>

Ramesh, K., Reddy, K. S., Rashmi, I., & Biswas, A. K. (2014). Porosity Distribution, Surface Area, and Morphology of Synthetic Potassium Zeolites: A SEM and N<sub>2</sub> Adsorption Study. *https://doi.org/10.1080/00103624.2014.929699*, 45(16), 2171–2181. <https://doi.org/10.1080/00103624.2014.929699>

Shaharoon, B., Al-Ismaily, S., Al-Mayahi, A., Al-Harrasi, N., Al-Kindi, R., Al-Sulaimi, A., ... Al-Abri, M. (2019). The role of urbanization in soil and groundwater contamination by heavy metals and pathogenic bacteria: A case study from Oman. *Heliyon*, 5(5), e01771. <https://doi.org/10.1016/j.heliyon.2019.e01771>

Shannon, R. D. (1976). Revised effective ionic radii and systematic studies of interatomic distances in halides and chalcogenides. *Acta Crystallographica Section A*, 32(5), 751–767. <https://doi.org/10.1107/S0567739476001551>

Shi, J., Yang, Z., Dai, H., Lu, X., Peng, L., Tan, X., ... Fahim, R. (2017). Preparation and application of modified zeolites as adsorbents in wastewater treatment. *Water Science and Technology*, 2017(3), 621–635. <https://doi.org/10.2166/wst.2018.249>

UNICEF and World Health Organization. (2015). *Progress on Sanitation and Drinking Water – 2015 update and MDG assessment*.

UNICEF and World Health Organization. (2019). *Progress on household drinking water, sanitation and hygiene 2000-2017. Special focus on inequalities. Launch version July 12 Main report Progress on Drinking Water, Sanitation and Hygiene*.

Vivar, M., Fuentes, M., Dodd, N., Scott, J., Skryabin, I., & Srithar, K. (2012). First lab-scale experimental results from a hybrid solar water purification and photovoltaic system. *Solar Energy Materials and Solar Cells*, 98, 260–266. <https://doi.org/10.1016/j.solmat.2011.11.012>



Vivar, M., Pichel, N., & Fuentes, M. (2017). Solar disinfection of natural river water with low microbiological content (10–103CFU/100 ml) and evaluation of the thermal contribution to water purification. *Solar Energy*, *141*, 1–10. <https://doi.org/10.1016/j.solener.2016.11.019>

Wang, Y., Jin, Y., Huang, Q., Zhu, L., Vivar, M., Qin, L., ... Cui, L. (2016). Photovoltaic and disinfection performance study of a hybrid photovoltaic-solar water disinfection system. *Energy*, *106*, 757–764. <https://doi.org/10.1016/j.energy.2016.03.112>

WHO, & UNICEF. (2017). *Progress on drinking water, sanitation and hygiene*.

Wu, M. J., Bak, T., Moffitt, M. C., Nowotny, J., Bailey, T. D., & Kersaitis, C. (2014). Photocatalysis of Titanium Dioxide for Water Disinfection: Challenges and Future Perspectives. *International Journal of Photochemistry*, *2014*, 1–9. <https://doi.org/10.1155/2014/973484>